

Published in final edited form as:

*J Immunol.* 2015 October 1; 195(7): 3248–3261. doi:10.4049/jimmunol.1500641.

## The Blood Transcriptome of Experimental Melioidosis Reflects Disease Severity and Shows Considerable Similarity with the Human Disease

Laura Conejero<sup>#,††</sup>, Krzysztof Potempa<sup>#§</sup>, Christine M. Graham<sup>#§</sup>, Natasha Spink<sup>\*</sup>, Simon Blankley<sup>§</sup>, Francisco J. Salguero<sup>\*\*\*</sup>, Rungnapa Pankla-Sranujit<sup>††</sup>, Prasong Khaenam<sup>††</sup>, Jacques F. Banchereau<sup>#</sup>, Virginia Pascual<sup>\*\*</sup>, Damien Chaussabel<sup>§§</sup>, Ganjana Lertmemongkolchai<sup>††</sup>, Anne O'Garra<sup>#§,##</sup>, and Gregory J. Bancroft<sup>#\*</sup>

<sup>\*</sup>Immunology and Infection Department, Faculty of Infectious and Tropical Diseases, London School of Hygiene & Tropical Medicine, London, UK. <sup>§</sup>The Francis Crick Institute, Mill Hill Laboratory, (formerly MRC National Institute for Medical Research), London, UK. <sup>\*\*\*</sup>School of Veterinary Medicine, University of Surrey, Guildford, UK. <sup>††</sup>The Centre for Research & Development of Medical Diagnostic Laboratories, Faculty of Associated Medical Sciences, Khon Kaen University, Thailand. <sup>#</sup>The Jackson Laboratory, Farmington, CT, USA. <sup>\*\*</sup>Baylor Institute for Immunology Research, Thousand Oaks, Dallas, Texas, USA. <sup>§§</sup>Damien Chaussabel, PhD, Director, Systems Biology Department, Sidra Medical and Research Center, Sidra Medical and Research Center, Al Nasr Tower, AL Corniche Street, Qatar Foundation | PO Box 26999 | Doha, Qatar. <sup>##</sup>NHLI, St. Mary's Hospital, Imperial College, London, UK

<sup>#</sup> These authors contributed equally to this work.

### Abstract

Melioidosis, a severe human disease caused by the bacterium *Burkholderia pseudomallei*, has a wide spectrum of clinical manifestations ranging from acute septicaemia to chronic localized illness or latent infection. Murine models have been widely used to study the pathogenesis of infection and to evaluate novel therapies or vaccines, but how faithfully they recapitulate the biology of human melioidosis at a molecular level is not known. Here, mice were intranasally infected with either high or low doses of *B. pseudomallei* to generate either acute, chronic or latent infection and host blood and tissue transcriptional profiles were generated. Acute infection was accompanied by a homogeneous signature associated with induction of multiple innate immune response pathways, such as IL10, TREM1 and IFN-signaling, largely found in both blood and

**Address for correspondence:** Dr Gregory J Bancroft Immunology and Infection Department, Faculty of Infectious and Tropical Diseases, London School of Hygiene & Tropical Medicine, London, UK. WC1E 7HT. **To whom correspondence should be addressed:** gregory.bancroft@lshtm.ac.uk +442079272361 .

<sup>††</sup>Current address: Vascular Biology & Inflammation Department, Centro Nacional de Investigaciones Cardiovasculares, Madrid, Spain.

**Author contributions:** GB, AOG, CG, LC conceived the experiments. GB, AOG, JB, VP, DC, GL oversaw the study and data analysis. LC, CG, NS and FJS performed the experiments. LC, KP, CG, SB, RP and PK, analysed the data. GB and AOG wrote the manuscript. All authors discussed results and commented on the manuscript.

Data and materials availability: The mouse microarray data is deposited in the Gene Expression Omnibus (GEO: GSE61106). <http://www.ncbi.nlm.nih.gov/geo/>

**Competing Interests:** All authors declare no competing interests.

tissue. The transcriptional profile in blood reflected the heterogeneity of chronic infection and quantitatively reflected the severity of disease. Genes associated with fibrosis and tissue remodelling, including MMPs and collagen, were upregulated in chronically infected mice with severe disease. Transcriptional signatures of both acute and chronic melioidosis revealed upregulation of iNOS in tissue, consistent with the expression of IFN- $\gamma$ , but also Arginase-1, a functional antagonist of the iNOS pathway, and was confirmed by immunohistochemistry. Comparison of these mouse blood datasets by pathway and modular analysis with the blood transcriptional signature of patients with melioidosis showed that many genes were similarly perturbed, including Arginase-1, IL10, TREM1 and IFN-signaling, revealing the common immune response occurring in both mice and humans.

---

## Introduction

Melioidosis, a severe human disease caused by infection with the environmental Gram-negative bacterium *B. pseudomallei* (1), is an important cause of community-acquired sepsis in Southeast Asia and Northern Australia where it is endemic. However, its known distribution is expanding with cases of melioidosis now being reported in numerous other countries (2). Infection results mainly from inhalation during the rainy season or from percutaneous inoculation (through direct contact with soil and water) (1). The severity of the disease has a wide spectrum of clinical manifestations. Acute fulminant septic illness is characterized by bacteraemia and induction of an extensive cytokine response (3, 4). In contrast, chronic localized infection is generally less severe with internal-organ abscesses and secondary foci in the lung, spleen, liver and skeletal muscle which persist and are difficult to eradicate (5). Sterilizing immunity does not occur and bacteria persist either subclinically in a latent form or as a chronic localized infection. Recurrent melioidosis is common and is usually due to relapse from a persistent focus of infection rather than to reinfection (6). Reactivation in some individuals has also been reported after decades of latency (7). Despite the increased research efforts since *B. pseudomallei* was classified by the USA Centers for Disease Control and Prevention as a Category B bioterrorism agent, the mechanisms of persistence and pathogenesis are still poorly understood and it is still unclear how *B. pseudomallei* can evade the immune response and cause significant human disease.

Murine models of melioidosis have been used extensively to study the immune responses induced following infection and to screen new vaccines and therapies (5, 8-10). Acute models, following either intravenous or the more physiologically relevant pulmonary route of *B. pseudomallei* infection, are characterized by the presence of bacteremia, neutrophil-dominant inflammation and uniformly rapid death (5, 8-10). We have also described a model of chronic melioidosis where granulomatous pathology, fibrosis and heterogeneity of disease progression are the main features within the infected animals (11). These models highlight the importance of neutrophil recruitment and IFN $\gamma$ -mediated macrophage activation (12) in host resistance, but how *B. pseudomallei* resists elimination by these cell mediated immune responses is not known. Together the acute and chronic mouse models share features resembling the heterogeneity of the clinical manifestations of human melioidosis, however, which of these models more closely resembles the human disease at a molecular as well as clinical level has not been addressed.

Whole genome transcriptional profiling has previously identified a blood signature in patients with septicemic melioidosis, which included genes related to inflammation, antigen processing and presentation, interferons, neutrophils and T cells (13-15). Transcriptional analysis of liver and spleen has been performed in a model of acute melioidosis by intravenous challenge (16) showing altered expression of genes involved in inflammation, TLR signaling and complement pathways. However, the transcriptional signature of acute and chronic melioidosis after infection via the airways, a natural route of transmission, has not been reported. In particular, a detailed molecular analysis of the global transcriptional response induced by infection with *B. pseudomallei* in different experimental models and how this compares with human disease has not been performed.

In this study we have performed whole genome transcriptional analysis of tissue and blood of mice following pulmonary challenge with *B. pseudomallei*, during acute and chronic infection, and compared this to the blood transcriptional profiles of patients with acute melioidosis in North East Thailand.

## Materials and Methods

### Bacteria and infection of mice

*B. pseudomallei* strain 576 was isolated from a patient with a fatal case of human melioidosis in Thailand, and was kindly provided by Dr. Tyrone Pitt (Health Protection Agency, London, UK). Frozen stocks were prepared as previously described (8). All procedures involving live bacteria were performed under ACDP containment level 3 conditions. Female C57BL/6 mice (Harlan Laboratories, Bicester, Oxon, UK) aged 6-10 weeks were used in accordance with the Animals (Scientific Procedures) Act 1986 and approved by the LSHTM Ethical Review Committee (70/6934). Aliquots of bacteria stocks were thawed, diluted in pyrogen-free saline (PFS) and administered intranasally in 50  $\mu$ L containing 2500 colony-forming units (CFU; acute model) or 100 CFU (chronic model) as previously described(11). Control uninfected mice received 50  $\mu$ L PFS.

### Preparation of mouse organs and determination of tissue and blood bacterial load

At different time points, mice were euthanized to determine the number of CFU in blood, lung, spleen and liver as described previously (11). The limits of detection were 50 CFU/organ or 20 CFU/mL of blood.

### Preparation of RNA from mouse whole blood, lung and spleen tissue

Mice were euthanized by terminal anaesthesia with pentobarbital (Euthatal; Merial, Essex, UK) and whole blood collected into Tempus™ tubes (Applied Biosystems, Paisley, UK); 1:2 ratio (blood:Tempus™ reagent). Samples were immediately vortexed to avoid blood clotting and stored at  $-80^{\circ}\text{C}$  until RNA extraction. Lung and spleen were harvested in 2 ml cold TRI-Reagent (RiboPure™ RNA kit, Life Technologies, Austin, TX), homogenized (Polytron PT 1600 E System; Kinematica AG; Luzern, Switzerland) and stored at  $-80^{\circ}\text{C}$  until RNA processing. The PerfectPure RNA Blood kit (5 PRIME, Hamburg, Germany) was used for whole blood RNA extraction, following manufacturer's instructions. Globin mRNA was depleted from 2  $\mu$ g total RNA blood samples using the GLOBIN-clear™ Mouse/rat kit

(Ambion, Life Technologies, Austin, TX). Lung and spleen RNA were extracted from tissue homogenates using the RiboPure™ Kit according to manufacturer's instructions. RNA concentration was determined (NanoDrop 1000, Thermo Scientific; Wilmington, USA) and RNA integrity values were assessed (LabChip GX, Caliper, USA). Samples with RNA integrity values  $>6$  were retained for further processing.

### Processing mouse RNA for microarray

RNA (300 ng/sample) was amplified (Illumina® TotalPrep RNA Amplification Kit (Applied Biosystems). cRNA (1.5 µg/sample) was hybridized overnight to Illumina Mouse Whole Genome WG6 V2 BeadChips (Illumina). BeadChips were washed, blocked, stained and then scanned on an Illumina iScan, as per manufacturer's instructions. Genome Studio 2.0 software (Illumina) was then used to perform quality control and generate signal intensity values.

### Mouse microarray data analysis

Raw background subtracted data from Genome Studio (Illumina) were generated and then analysed using GeneSpring GX 12.1 software (Agilent Technologies). Signal values were set to threshold level 10, log<sub>2</sub> transformed, and normalized using a 75<sup>th</sup> percentile shift algorithm. Next, per-transcript normalization was applied by dividing each messenger RNA transcript to the median intensity of all the samples. Transcripts were filtered out if at least 10% of the samples failed to pass a 'present' flag cut off set at 0.99 (detection  $p$ -value  $> 0.01$ ). The above normalized and quality controlled data were used to identify differentially expressed transcripts having at least two-fold expression value changes from the median of all transcripts in at least 10% of all samples, which passed Mann-Whitney test with Benjamini-Hochberg false discovery rate correction between infected and uninfected mice ( $p < 0.01$ ). Heatmap dendrograms of differentially expressed transcripts were generated by clustering with Pearson Uncentered distance metric and the Average Linkage rule on transcripts, unless otherwise stated. All data collected and analysed adhere to the Minimal Information About a Microarray Experiment (MIAME) guidelines. Mouse microarray data were deposited in the Gene Expression Omnibus (GEO: GSE61106). For Figures 1 and 3, significant transcript lists were identified by stringent statistical filtering comparing infected to uninfected mice (Mann-Whitney test plus Benjamini-Hochberg correction  $p < 0.01$ ) on data normalized to the median of all transcripts across all samples and passing a detection value ( $p < 0.01$ ) and 2-fold expression value across at least 10% of samples within GeneSpring GX12.1 statistical software.

### Molecular distance to health

Weighted molecular distance to health/uninfected (MDTH) was calculated as previously described (15). Molecular distance to health/uninfected (MDTH) was determined for each dataset by computing the 'molecular distance' between each *B. pseudomallei* infected sample in relation to all uninfected control samples. Qualifying genes differed from the average baseline expression by at least 200 and 2 standard deviations. Nonparametric one-way ANOVA (Kruskal-Wallis) with Dunn's post-hoc test was applied between sample groups  $p < 0.01$  (\*\*),  $p < 0.001$  (\*\*\*) and  $p < 0.0001$  (\*\*\*\*) between uninfected group are indicated. Significant transcripts (811) were identified by comparing *B. pseudomallei*

infected mice without bacteraemia (n=7) to uninfected (n=8) (Mann-Whitney test plus Benjamini-Hochberg correction  $p < 0.01$ ) on data normalized to the median of all transcripts across all samples and passing a detection value ( $p < 0.01$ ) and 2-fold expression value across at least 10% of samples. Lesion scores were applied to generate a supervised heatmap of the identified transcripts. Bacterial counts from spleens were allocated into two groups according to the presence or absence of visible lesions.

### Canonical pathway and immune gene analysis

Ingenuity Pathway Analysis (IPA, Qiagen, [www.ingenuity.com](http://www.ingenuity.com)) knowledge base was used to identify statistically significant pathways (Fisher's exact test,  $p < 0.05$ ) associated with differentially expressed transcripts ( $p < 0.01$  after Mann-Whitney test and Benjamini-Hochberg correction) following *B. pseudomallei* infection of blood or tissues (lung, spleen). A list of 3,468 genes associated with an immune GO function was generated by search within IPA (19 March 2014) and the Mouse Genome Database (MGD) at the Mouse Genome Informatics website, The Jackson Laboratory, Bar Harbor, Maine. World Wide Web (URL: <http://www.informatics.jax.org>) (30 March 2014).

### Immunohistochemistry

At necropsy, lung and spleen samples were fixed in 10% formalin and routinely processed for histopathology. Four  $\mu\text{m}$  thick sections were stained with haematoxylin and eosin or used for immunohistochemistry (IHC). Sections for IHC were dewaxed and hydrated in Tris Buffered Saline solution (TBS) (0.005 M Tris, pH7.6, 0.85% w/v NaCl). For detection of Arginase-1, sections were incubated for 5 min with 1% sodium dodecyl sulphate in TBS before endogenous peroxidase activity was quenched with a methanol/hydrogen peroxide block (BDH) for 15 min. Slides were assembled into Shandon cover plates (Shandon, USA) and incubated subsequently at room temperature with avidin/biotin block (Bloxall, Vector Laboratories, UK) for 10 min, M.O.M Ig Block (Vector M.O.M Immunodetection Kit, Vector Laboratories) for 1 h, Mouse anti Arginase I antibody (BD Transduction Laboratories, UK) 1/250 in M.O.M diluent for 45 min, M.O.M. biotinylated anti mouse IgG (Vector Laboratories) for 10 min and Avidin-biotinperoxidase complex (ABC, Vector laboratories) for 30 min and washed three times with TBS between incubations. Sections for iNOS detection had their endogenous peroxidase activity quenched followed by an epitope unmasking with Dako pH 9.0 buffer (Dako Cytomation, UK) for two periods of 5 min at 800 W in microwave and sequential incubation with avidin biotin block, normal serum block for 30 min, rabbit anti-iNOS/NOS II polyclonal antibody (Millipore, UK) 1/500 or in TBST for 1 h, goat anti rabbit biotinylated secondary antibody (Dako) 1/1000 in TBS for 30 min and ABC. Primary antibodies were substituted by homologous IgGs (isotype control) as negative technique controls. Samples were imaged using a Zeiss axioplan 2 microscope (Carl Zeiss Ltd, Welwyn Garden City, UK) fitted with a Retiga 2000R Fast CCD camera (QImaging, Marlow, UK) using Volocity software from Improvision.

### Human microarray data analysis

Whole blood transcriptional microarray data (Illumina Hu6 V2 Beadchips) from our already-described Training and Test cohort of melioidosis patients and healthy controls (15) were reanalysed. The Training group contained 11 patients and 10 healthy controls, while

the Test group contained 13 patients and 9 healthy controls. Differentially expressed transcripts were identified from quality control filtered data (transcripts detected in at least 10% of all samples at detection  $p$ -value  $< 0.01$  and passing a filter of two-fold median intensity value and 200 intensity units across all samples) by Mann-Whitney test and Benjamini-Hochberg false discovery rate correction between patients and healthy controls ( $p < 0.01$ ) as above.

### Human-mouse orthologs

Of the genes represented in the Illumina whole genome mouse arrays (WG6 V2), 19,945 had annotated Entrez IDs. Of the 20,268 annotated human genes, 15,976 had mouse orthologs based on the IPA knowledge base. For the 1292 genes common between human Training and Test Sets that were significantly changed in human melioidosis, 1131 had mouse orthologs, which were included in subsequent analysis.

### Modular analysis

To compare human and mouse data at the modular level, we used the previously described Affymetrix-derived human module system (17) and translated the module lists to accommodate mouse genes based on Entrez IDs. The 2,051 Illumina/AffyIDs used to compute the Affymetrix Modules were entered into IPA, resolving 1,832 genes common to the Human Illumina Hu6 V2 and Mouse WG6 V2 arrays (17). Raw values for the common 1,832 human-mouse genes were used to generate module heatmaps. Percentages of significantly expressed upregulated or downregulated genes (Student's  $t$ -test,  $p < 0.05$  comparing infected and uninfected) in each module are represented by colored intensity areas.

## Results

### IL10 and TREM1-signaling pathways and immune genes are perturbed in blood and lung upon acute infection of mice with *B. pseudomallei* as shown by transcriptional analysis

Our initial aim was to investigate whether the blood transcriptional signature of mice infected via the airways with *B. pseudomallei* could reflect transcriptional changes in the lung. Genomewide transcriptional profiles were generated from blood and lung samples from acutely infected C57BL/6 mice at days 1 and 3 post intranasal infection with 2500 CFU *B. pseudomallei* 576. Typically, their bacterial load in the lung at day 2 was around  $10^6$  CFU and increased up to  $10^8$  CFU by day 3, whereas  $10^3$  CFU were detected in the blood by day 2 and these mice usually die at day 4 postinfection (data not shown). Unsupervised analysis of blood and lung samples showed that the transcriptional profile of the groups segregated according to infection as shown by Principal Component Analysis (PCA). (Fig. S1). Statistical filtering ( $p < 0.01$  Mann-Whitney, Benjamini-Hochberg correction of infected versus uninfected mice using GeneSpring analysis) resulted in two main dendrogram clusters based on similarity of gene expression, showing 1325 and 2041 transcripts differentially expressed in the blood and lung, respectively, of infected as compared to uninfected mice at day 1 (Fig. 1A). A greater number of differentially expressed genes consisting of 4810 and 4076 transcripts was observed respectively in the blood and lungs of mice at day 3 postinfection compared to uninfected controls (Fig. 1A). The top 5 Ingenuity

Pathway Analysis (IPA) Canonical Pathways upregulated at both time points in blood and lung were highly enriched for Granulocyte Adhesion and Diapedesis, IL10 and TREM1-signaling and other pathways involved in innate immunity (Fig. 1B). The IFN-signaling pathway was one of the top upregulated pathways in the blood but not in the lung at the early time point. Other upregulated pathways included Hepatic Fibrosis and Acute Phase Response. The top 5 downregulated pathways in both blood and lung at days 1 and 3 largely consisted of B- and T-cell-associated genes (Fig. 1C). The transcriptional signature showed 561 transcripts were common to the blood and lung at day 1 and represented 404 genes identified by IPA (Fig. 1D). The 1618 common transcripts detected in both blood and lung at day 3 postinfection represented 1236 genes (Fig. 1E).

Further analysis of blood and lung genes associated with acute infection, as defined by both the IPA Knowledge Base and by Gene Ontology (GO) resources available through the Mouse Genome Database, revealed perturbation of a significant number of genes not obviously associated with the immune response (Fig. 2A). In blood at day 1, of 584 upregulated genes, only 267 (46%) were associated with the immune response, and this was increased at day 3 to 473 out of 1522 (31%) total upregulated genes. Similarly, of 829 total upregulated genes in lung at day 1, only 441 (53%) genes were involved in immune function. This increased to 716 immune response genes out of a total of 1795 (40%) genes at day 3 postinfection in the lung. Of 327 genes downregulated in blood at day 1 postinfection, 106 (33%) were associated with immune function and this was increased to 418 (25%) genes associated with immune function out of 1661 at day 3 postinfection. The functional type of these genes are shown in Fig. 2B. A substantial set of genes was common and similarly perturbed in both blood and lung and day 1 and also at day 3 postinfection (Fig. 2C and 2E).

Of the genes that were altered in response to infection at day 1, 507 were only expressed in the blood of which 166 (11%) were immune genes, 1028 were only expressed in the lung, of which 349 (34%) were immune genes, whereas 404 were coexpressed in blood and lung of which 207 (51%) were immune genes (Fig. 2D). These numbers were increased at day 3 postinfection with 1947 genes expressed in blood of which only 407 (21%) were immune genes, 2018 were unique in the lung of which 544 were immune genes and 1236 coexpressed in blood and lung, of which 485 (27%) were immune genes (Fig. 2F). Upregulated genes common to both blood and lung at days 1 and 3 after infection included a large number of chemokines and cytokine genes including IL27, IL1, TNF and IFN-inducible genes, matrix metalloproteases (MMPs), Caspase and ADAM family members. There is altered expression of genes not annotated by IPA/GO as involved in immunity, suggesting these are either physiological changes upon infection, or have an underappreciated role in immunity.

### **The blood transcriptome of mice chronically infected with *B. pseudomallei* reflects the disease severity in the tissue**

We have established a mouse model of chronic melioidosis where mice are intranasally infected with a low dose of the organisms (11), which together with the acute respiratory models described earlier in this manuscript (1, 2) may represent the spectrum of pathological

findings observed in patients with this disease (5). Severity at any one time point, ranges from mice with latent infection with no signs of disease, but from which bacteria cannot be detected in the spleen, through to active infection with the presence of high levels of bacterial burden and severe lesions in the spleen (11). To determine whether the blood transcriptome reflects the heterogeneity of disease progression, blood was harvested from chronically infected mice and RNA was extracted and processed for microarray analysis. Unsupervised PCA analysis of blood transcripts passing detection limits ( $p < 0.01$ ) showed that samples from uninfected mice clustered together with those with latent infection and away from mice with either moderate clinical severity (Grade 1-2) or those with clinical severity grade 3 (fig. S1). Upon statistical filtering ( $p < 0.01$  Mann-Whitney, Benjamini-Hochberg correction of infected versus uninfected mice using GeneSpring analysis) segregated mice into groups, either expressing a strong signature, a weak signature or no signature of over and underexpressed transcripts, as compared to uninfected controls (Fig. 3A). In keeping with the PCA analysis, some mice, although infected showed a blood signature which clustered with that of uninfected controls. Upon analysis of gross pathology some mice were found to have no detectable lesions at this time point and were latent. Mice with detectable lesions, ranging in severity from 1 to 3 showed a strong transcriptional blood signature, confirmed quantitatively using the Weighted Molecular Distance to Health (MDTH) algorithm (15) (Fig. 3B). This quantitation using MDTH for measuring the extent of the blood signature correlated with the extent of disease severity based on the spleen lesion score (Fig. 3C). A blood transcriptional signature statistically distinct from that of uninfected mice was detected even in the absence of bacteraemia (Fig. 3D). Mice that were chronically infected with low-dose *B. pseudomallei* could be grouped according their splenic bacterial burden; latent mice (no detectable bacteria); emerging mice (low levels of bacteria with no clinical illness); mice with active disease (high bacterial burdens and clinical disease) (Fig. 3E). As shown in the blood splenic transcriptional signatures again correlated with disease severity (Fig. 3F, G and H).

### **Blood transcriptional profile of chronically infected mice shows similarity to that of acute infection**

Using canonical IPA, many similarities between the blood transcriptome of acute and chronic infection were observed, with the top 5 pathways of upregulated genes comprising Granulocyte Adhesion and Diapedesis, IFN-signaling and TREM1-signaling (Fig. 4A and B). The top 5 downregulated pathways in the blood of both chronically and acutely infected mice consisted of genes related to B Cell Development (Fig. 4C and Fig 1C).

The splenic signature of chronic infection was also dominated by the Granulocyte Adhesion and Diapedesis pathway, but additionally included Heme Biosynthesis II, LXR/RXR Activation and Hepatic Fibrosis in the top 5 upregulated IPA pathways (Fig. 4B). The downregulated genes in the spleen of mice after chronic infection were dominated by those involved in T-cell responses (Fig. 4C).

Of the upregulated genes in blood, 327 (42%) were immune response genes out of a total of 774, whereas 532 (34%) out of 1571 were upregulated immune response genes in the spleen (Fig. 4D). Of the 496 downregulated genes in the blood, 144 (29%) were immune response

genes, whereas 371 (31%) immune response genes out of 1185 were downregulated in the spleen. The functional type of genes altered during chronic infection is shown in Fig. 4E. Many were common and similarly perturbed in both blood and spleen during chronic infection (Fig. 4F).

Comparison of the signatures of chronic blood and spleen showed: 502 unique to the blood of which 141 (28%) were immune genes; 768 genes were common in blood and spleen, of which 331 (43%) were immune genes; and 1988 were unique to the spleen of which 572 (29%) were immune genes (Fig. 4G). A large number of the immune genes common to blood and spleen of chronically infected mice again included chemokines, and cytokine genes such as IL27, IL1, TNF and IFN-inducible genes, Caspase and ADAM family members, (Fig. S2). Consistent with the histological evidence of fibrosis in chronically infected spleens (11), we observed upregulation of numerous genes associated in other systems with fibrosis and tissue remodelling (18) (19), although these genes were invariably expressed to a greater extent in tissue than blood (Fig. 4H). These included collagen-1, multiple MMPs (MMP-2,3,8,9,10,12,13,14 and 25), IL-1 $\beta$ , IL-6, Connective Tissue Growth Factor (CTGF), chemokines (CCL2,CCL4, CCL6 and CCL8) as well as the Chitinase-like protein BRP-39 (Chitinase 3-like1) and Fizz 2 (RELM $\beta$ ) (Fig. 4H) (Fig S2).

### **Similar immune response pathways and modules are revealed in the blood transcriptome of mice and humans infected with *B. pseudomallei***

To determine which of the mouse models of melioidosis most recapitulated the human disease, we then compared the immune signatures of blood and tissue in mice acutely or chronically infected with *B. pseudomallei*, with those of human melioidosis cases (15). We first determined the common sets of genes expressed in our Training and Test set human blood samples (1292 genes; Fig. 5A) from patients with *B. pseudomallei*, who were admitted to hospital with blood culture proven melioidosis (15). Consideration of all genes that were altered in each data set revealed that 26.9% of the genes perturbed in human melioidosis were also similarly regulated in the mouse models (Fig. 5B). However, the highest level of similarity with human was observed at day 3 post acute infection of mice (Fig. 5B). Of the 26.9% genes commonly affected in both human and mouse blood, of those upregulated 118 were immune, 90 were nonimmune functionally (Fig. 5C). Of the 118 upregulated genes, 50 were commonly affected in all mouse models and the human disease, including arginase 1, cytokine genes, as well as MMPs, and TLRs (fig. S4). The remainder of upregulated immune genes in the blood of melioidosis patients was similarly affected in at least one of the mouse models of *B. pseudomallei* infection, again with the acute day 3 transcriptome showing the greatest similarity (fig. S4).

IFN $\gamma$  is essential for resistance against infection with *B. pseudomallei* in mice, and is produced by human NK and T cells *in vitro*, but the role of Type I IFNs is not known (20, 21). Consistent with the presence of IFN $\gamma$ , we observed significant upregulation of iNOS mRNA in the tissues of both acute and chronically infected mice (Fig. 5D). This was confirmed by immunohistochemistry, where iNOS was shown to be clearly localised to the macrophage rich zones of acute lung and chronic spleen lesions (Fig. 5E and 5F), indicating the presence of M1 or classically activated macrophages. Expression of iNOS mRNA was

however not detectable in the blood of infected mice or humans (Fig. 5D). Incongruously, Arginase-1, a functional antagonist of the iNOS-mediated microbicidal pathway and a prototypic M2 or alternatively activated macrophage marker, was highly expressed at the mRNA level in the tissue of acute and chronically infected mice (Fig. 5D). In keeping with the elevated levels of Arginase-1 mRNA, Arginase-1 protein was also observed at high levels in the lung and spleen of acute and chronically infected mice respectively (Fig. 5E and 5F). Arginase-1 protein was predominantly observed in neutrophils in acute lung lesions, whereas in chronically infected spleen samples it was observed within macrophages. Together with the increased expression of Ym-1 mRNA, this suggests that in chronic infection, both M1 and M2 macrophage populations are induced in response to persistent exposure to *B. pseudomallei* with the latter potentially contributing to the tissue repair and fibrosis observed in these lesions. Of note, in contrast to iNOS, Arginase-1 mRNA was highly expressed in the blood of infected mice and humans (Fig. 5D).

IPA was then used to select the top 25 ranked pathways across the human and mouse blood datasets based on their average  $p$ -value (Fig. 6A – where the total 109 pathways significant at  $p < 0.05$ , score 1.31, averaged over the blood transcriptome of human melioidosis and mouse days 1 and 3 acute and chronic melioidosis). The dataset-specific  $p$ -values are summarized in Fig. 6A and include IL10-signaling, TREM1-signaling, Pattern-Recognition Receptors in Recognition of Bacteria and Viruses and TLRs, corroborating our previous IPA analyses. Genes associated with IFN-signaling were now also observed in both human and mouse datasets using this approach (Fig. 6A). Similar results were obtained by looking at top 10 pathways associated with each dataset (fig. S3).

IFN $\gamma$  itself was shown to be upregulated in the blood (Fig. 6B), but only in chronically infected mice, whereas Type I IFNs were not. Analysis of expression of genes annotated across all IFN-related IPA-signaling pathways showed clear induction of genes in the blood of acute and chronically infected mice, involving both Type I and Type II signaling (Fig. 6B). Comparison of these results with the blood of patients with acute melioidosis showed several genes in common to the murine response including SOCS1, STAT1, STAT2, IFITM1 and TAP1 (Fig. 6B).

We then compared gene expression profiles in infected mice and humans using a modular data-mining strategy, which analyses clusters of genes that are coordinately regulated (17, 22). The 28 human modules contained from 2 to 192 genes per module, corresponding to 2 to 183 mouse genes with a range of 75-100% mouse to human homology, depending on the module examined. Modular analysis of our original human training and test sets of human melioidosis samples showed clear changes in gene expression in a total of 18 distinct functional modules with increased expression of IFN (M3.1), inflammation (M3.2 and M3.3), neutrophil (M2.2) and myeloid (M2.6) modules and decreased expression of B- and T-cell modules (Fig. 7). Of these, 5 of the modules showing upregulation of IFN, inflammation, neutrophil and myeloid genes were similarly altered in the blood of all of the mouse models of acute and chronic melioidosis. Whilst B-cell-associated genes were shown to be downregulated in both acute and chronic melioidosis, the downregulated T-cell-associated genes were only apparently downregulated during acute disease in keeping with the top 10 pathways shown to be downregulated by IPA (fig. S3), although closer analysis of

each module demonstrates a number of T-cell-associated genes downregulated at all stages of mouse melioidosis that are common with human disease (Fig. 7). These data demonstrate highly conserved changes across both mouse and human responses in genes associated with IFNs (e.g. IFITM1, SERPING1, CXCL10), neutrophils (e.g. Arginase 1, MMP9, LCN2), B cells (e.g. FCRLA, VPREB3, BCL11A) and T cells (CCR7, BCL11B, FAIM3) (Fig. 7). Thus, by several different analytical approaches, the host response to *B. pseudomallei* was dominated by upregulation of genes involved in IFN-signaling, phagocyte biology and inflammation and downregulation of genes involved in B- and T-cell responses, which was conserved between mice and humans. A number of modules showed discordancy between human disease and the experimental models of melioidosis: one myeloid gene module (M1.5) was not globally similar between mouse and human, overrepresented only in the mouse models (Fig. 7). More detailed inspection of the actual list of genes in that module showed that 20 out of 77 of the genes were upregulated in both mouse and human. Discordancy also included underexpression of genes encoding ribosomal proteins in humans, which were either not perturbed or rather overrepresented in the mouse; and six modules consisting of nonannotated genes underrepresented in human disease but not in the mouse models.

### **Network level analysis of common mouse and human *B. pseudomallei* associated transcriptional signatures**

Gene and network level analysis of the 348 common mouse and human *B. pseudomallei* associated genes showed 179 directly interacting genes, which included members of modules associated with B cells (M1.3) and T cells (M2.8) which were downregulated versus those associated with Inflammation (M3.2 and M3.3), Neutrophils (M2.2), Myeloid (M2.6) and IFN (M3.1) genes, which were upregulated (Fig. 8).

## **Discussion**

Melioidosis is an increasingly important cause of severe bacterial infection in tropical countries, requiring intense and prolonged antibiotic treatment and for which there is no effective vaccine. Following exposure to *B. pseudomallei* a diverse range of clinical outcomes occurs, ranging from prolonged periods of latency to chronic active disease and acute, lethal sepsis. To further our understanding of immunity and pathogenesis of this infection, we have applied whole genome transcriptional microarray to blood and tissues from mouse models, which reflect each of these stages of infection, and compared these profiles to those of melioidosis patients in N.E. Thailand. We show that the blood transcriptome in mice infected with *B. pseudomallei* accurately reflects disease severity in latent, acute and chronic infection and that the transcriptional signature of disease in mice has substantial similarity to that observed in human melioidosis.

Our initial experiments used an established model of acute pneumonia and lethal sepsis following high dose intranasal challenge of mice with a virulent strain of *B. pseudomallei*. Transcriptional array analysis of blood showed clear and extensive transcriptional responses in infected but not control mice within 24 hrs, which increased by 72 hrs. This included upregulation of numerous proinflammatory gene pathways, consistent with a previous report

following intraperitoneal infection (16). There was also coordinated downregulation of genes involved in both B and T lymphocyte development and function, possibly due to the egress of these cells from the circulation or apoptosis, as we have previously described in human disease (15, 22, 23). To date, our understanding of events in the lung leading to severe pneumonia after exposure to *B. pseudomallei* via the airways have been limited. Wiersinga and colleagues, using a 33 gene probe array reported induction of several proinflammatory cytokines and chemokines in the lung and bronchoalveolar lavage of infected mice (24). Our whole genome array approach now shows the full scale of the host transcriptional changes in the lung during the development of acute pneumonia. Within 24 hours of exposure to bacteria, some 1400 genes showed altered levels of transcription, and over 3200 genes at the later time point of 72 hrs when clear signs of systemic illness (such as weight loss and bacteraemia) were evident. Most of these genes were not annotated as being directly involved in the immune response using a combination of the genes listed in both GO and IPA, presumably reflecting the massive physiological changes occurring during this time. Functional gene types including GPCR, kinases, phosphatases and transcriptional regulators were annotated in both immune and nonimmune response gene families, with an overabundance of GPCRs and transcriptional regulators associated with the immune response genes after infection. Consistent with the influx of different leucocytes into the lungs (25), expression of multiple genes encoding chemokines, (including CCL2, CCL7 and CXCL2), cytokines (IL6, IL18 and TNF) and the immunoregulatory pathway for IL10 were increased. Increased expression of multiple genes involved in pattern recognition were also observed, consistent with the important role of MyD88/TLR and other innate recognition pathways to resistance against *B. pseudomallei* (26). Several gene expression pathways were found in common between lung and blood of infected mice including, TREM1 and IL10-signaling and Granulocyte Adhesion and Diapedesis.

Although acute infection of mice is frequently used to study immunity to *B. pseudomallei*, (2) it does not allow investigation of the latent or chronic phases of melioidosis also seen in humans living in endemic areas. To address this, we established a new model using low-dose intranasal challenge into genetically resistant mice which leads to prolonged periods of latency but which eventually progresses in all animals to an active chronic infection, characterized by extensive granulomatous lesions in the spleen containing numerous macrophages and lymphocytes (11). Enumeration of the bacterial burden in the spleen of infected animals throughout this process showed three discrete groups; i) those with undetectable bacteria and no tissue lesions (latent), ii) those with low levels of bacteria but no lesions (emerging), and iii) those with high levels of bacterial burden and obvious lesions (active). Unlike the coordinated and homogenous transcriptional response seen in the acute model, blood from chronically infected mice showed a pronounced heterogeneity in gene expression, which correlated directly with these three stages of infection. A weighted MDTH method showed that during the latent phase of infection, there is no appreciable change in host gene expression above the baseline of uninfected animals, presumably a reflection of the low numbers of bacteria in the tissues not showing an overt immune response. This heterogeneous pattern of gene expression was also observed in the spleen, the main target organ of chronic infection, and again reflected the degree of disease severity as shown by spleen lesion score. The transcriptional signature of severe chronic disease

included expression of multiple genes associated in other systems with tissue remodelling and fibrosis, including MMPs and Collagen, at high levels in the tissue and to a lesser extent in the blood, in keeping with our previous report of the prominent fibrosis observed in lesions of chronically infected mice (11).

In many bacterial infections including melioidosis, a significant proportion of individuals present with signs of acute disease due to the presence of foci of bacteria in their tissues but are blood culture negative (15). The inability to confirm the identity of the pathogen poses considerable challenges to the management of these patients and new methods to indicate the presence of infecting organisms are needed. Here we show in mice, that blood transcriptional arrays were sufficiently sensitive to indicate the presence of *B. pseudomallei* lesions in tissues such as liver and spleen, in the absence of bacteraemia. This most likely reflects the migration of activated cells from infected tissues into the circulation and/or the activation of blood leucocytes by subcellular fragments of bacteria, such as LPS or cell wall components, released from the lesions. These data suggest that transcriptional profiling may be a useful tool in blood culture negative patients for confirming the presence of infection, predicting the risks of dissemination and systemic illness and in identifying those likely to relapse following antibiotic treatment by indicating the presence of residual tissue foci of infection.

Using a combination of analytical methods to interrogate gene expression profiles, including GO, IPA, pathways and modular approaches, we evaluated the similarity between mouse and human blood datasets associated with *B. pseudomallei* infection. We first identified a common 1292 gene reference list from two sets of human melioidosis patients (15) that comprised 1131 murine orthologs and then calculated the similarity between human and mouse datasets provided by our different models of acute and chronic *B. pseudomallei* infection. A 26.9% overlap was observed in the combined acute (day 1 and day 3) and chronic *B. pseudomallei* infection mouse models for the common 1292 genes perturbed in human melioidosis. Furthermore, using a focused pathway or modular approach highlighted several individual top pathways that strongly correlated in human and mouse. IPA pathways with the highest averaged overlap of human genes present across mouse pathways included upregulation of Granulocyte Adhesion and Diapedesis, Crosstalk between Dendritic Cells and Natural Killer Cells, IFN-signaling and IL10-signaling, and downregulation of genes associated with B-cell and T-cell pathways. Similarly, infectious disease-based gene modules highlighted that several of them are similarly activated or repressed in human and mouse models. These included the upregulated modules associated with IFN-inducible, inflammation, neutrophil and myeloid genes, and the downregulated modules associated with B-cell and T-cell genes. Surprisingly a prominent finding revealed by our transcriptomic analysis of both infected mice and humans was the prominent up-regulation in both blood and tissue of Arginase-1, which led us to investigate and confirm its presence at the protein level within the lesions of infected mice. Arginase-1 is known to antagonise the iNOS microbicidal pathway and to inhibit T cell immunity in other infections (27) (28) (29) (30) and thus may be a contributing factor to why in *B. pseudomallei* infection sterilising immunity is rarely achieved.

It has been suggested that mouse models poorly mimic human inflammatory diseases (31). This prompted us to evaluate the similarity of mouse and human blood datasets associated with *B. pseudomallei* using the methodology adopted by Seok et al. Using the 1292 human gene reference list comprising 1131 murine orthologs we calculated the similarities between human and mouse datasets by the same approach as Seok et al (Pearson correlation,  $R^2$ ). We obtained  $R^2$  correlations of 0.95 (human Pankla Test), 0.17 (mouse blood day 1), 0.15 (mouse blood day 3) and 0.15 (mouse blood chronic) when fold-change values of patients to healthy within the Human Pankla Training dataset were taken. The weak correlation values between 0.15 and 0.18 are higher than the human-mouse correlations of 0 to 0.08 reported by Seok et al. In contrast, the murine mouse models of melioidosis strongly correlated with each other ( $R^2 = 0.60-0.62$ ). Using this approach, we obtained strong ( $R^2 = 0.95$ ) correlation values for human-human comparisons and weak ( $R^2 = 0.14-0.18$ ) correlations for human-mouse comparisons. Seok et al., however, reported stronger ( $R^2 = 0.49$ ) human-mouse correlations in individual top pathways, indicating that certain key genes and pathways illustrate similarities between mouse models and human disease, and could help to develop improved animal models. Indeed, our unbiased approach using complementary bioinformatic tools, including GO, pathway and modular analyses, demonstrates that there are clear similarities between mouse and human immune responses, as measured by the blood transcriptome, to *B. pseudomallei* infection. Furthermore of the 348 genes commonly perturbed between mouse and human, 51% were predicted to be directly interacting, the majority of which were involved in immune responses.

Taken together, we show that the level at which one compares human-mouse transcriptional datasets can lead to disparate conclusions regarding the similarity of mouse models to human disease. Perfect correlation between murine and human data should not be expected given the nature of the experimental versus clinical conditions. With the human dataset there is heterogeneity at the individual level, not only in terms of underlying genetic makeup of the individuals but also with regard to the dose received of infectious agent, variance in the virulence of the pathogen as well as variation in the time of sampling during the course infection all of which cannot usually be determined in humans under noncontrolled conditions. In addition, there is additional heterogeneity according to the time of initiation of treatment and type of treatment. In contrast, greater control is possible over these variables (pathogen strain, pathogen dose, mouse strain, time after infection and balanced control of experimental groups) in murine models that allows for the in-depth analysis of perturbed gene expression.

Thus, while comparisons of human and mouse models of disease at the level of a global list of significantly expressed genes from human disease models may poorly correlate with expression profiles from mouse disease models, the identification of key genes or pathways shared in the response in murine and humans may reveal known and potentially novel immune response mechanisms following infection by a pathogen and may help to identify biomarkers relevant to the interplay between host and pathogen. The development of more focused approaches such as modular analysis developed in diverse mouse models is needed for interpreting and further developing animal models of human disease. Our data not only provide new information on the pathogenesis of this infection but also demonstrate that a complementary set of bioinformatics approaches can provide valuable and novel insight into

the conserved response pathways in mouse and man, validating mouse models of human disease and providing approaches to improve them.

## Supplementary Material

Refer to Web version on PubMed Central for supplementary material.

## Acknowledgements

We thank R. Gilbert and the LSHTM BSF for animal husbandry. We thank A Sesay, H. Jani and the High Throughput Sequencing Facility, NIMR, for microarray.

**Funding:** This project and KP were funded by the ERC 204682, TB-PATH. AOG and CMG funded by the Medical Research Council, UK, MRC grant U117565642.

## References

1. Wiersinga WJ, van der Poll T, White NJ, Day NP, Peacock SJ. Melioidosis: insights into the pathogenicity of *Burkholderia pseudomallei*. *Nature reviews. Microbiology*. 2006; 4:272–282. [PubMed: 16541135]
2. Wiersinga WJ, Currie BJ, Peacock SJ. Melioidosis. *The New England journal of medicine*. 2012; 367:1035–1044. [PubMed: 22970946]
3. Friedland JS, Suputtamongkol Y, Remick DG, Chaowagul W, Strieter RM, Kunkel SL, White NJ, Griffin GE. Prolonged elevation of interleukin-8 and interleukin-6 concentrations in plasma and of leukocyte interleukin-8 mRNA levels during septicemic and localized *Pseudomonas pseudomallei* infection. *Infection and immunity*. 1992; 60:2402–2408. [PubMed: 1375198]
4. Lauw FN, Simpson AJ, Prins JM, Smith MD, Kurimoto M, van Deventer SJ, Speelman P, Chaowagul W, White NJ, van der Poll T. Elevated plasma concentrations of interferon (IFN)-gamma and the IFN-gamma-inducing cytokines interleukin (IL)-18, IL-12, and IL-15 in severe melioidosis. *The Journal of infectious diseases*. 1999; 180:1878–1885. [PubMed: 10558944]
5. White NJ. Melioidosis. *Lancet*. 2003; 361:1715–1722. [PubMed: 12767750]
6. Limmathurotsakul D, Chaowagul W, Chierakul W, Stepniewska K, Maharjan B, Wuthiekanun V, White NJ, Day NP, Peacock SJ. Risk factors for recurrent melioidosis in northeast Thailand. *Clinical infectious diseases : an official publication of the Infectious Diseases Society of America*. 2006; 43:979–986. [PubMed: 16983608]
7. Mays EE, Ricketts EA. Melioidosis: recrudescence associated with bronchogenic carcinoma twenty-six years following initial geographic exposure. *Chest*. 1975; 68:261–263. [PubMed: 1149556]
8. Haque A, Easton A, Smith D, O'Garra A, Van Rooijen N, Lertmemongkolchai G, Titball RW, Bancroft GJ. Role of T cells in innate and adaptive immunity against murine *Burkholderia pseudomallei* infection. *The Journal of infectious diseases*. 2006; 193:370–379. [PubMed: 16388484]
9. Tan GY, Liu Y, Sivalingam SP, Sim SH, Wang D, Paucod JC, Gauthier Y, Ooi EE. *Burkholderia pseudomallei* aerosol infection results in differential inflammatory responses in BALB/c and C57Bl/6 mice. *Journal of medical microbiology*. 2008; 57:508–515. [PubMed: 18349373]
10. Titball RW, Russell P, Cuccui J, Easton A, Haque A, Atkins T, Sarkar-Tyson M, Harley V, Wren B, Bancroft GJ. *Burkholderia pseudomallei*: animal models of infection. *Transactions of the Royal Society of Tropical Medicine and Hygiene*. 2008; 102(Suppl 1):S111–116. [PubMed: 19121670]
11. Conejero L, Patel N, de Reynal M, Oberdorf S, Prior J, Felgner PL, Titball RW, Salguero FJ, Bancroft GJ. Low-dose exposure of C57Bl/6 mice to *Burkholderia pseudomallei* mimics chronic human melioidosis. *The American journal of pathology*. 2011; 179:270–280. [PubMed: 21703409]
12. Breitbach K, Klocke S, Tschernig T, van Rooijen N, Baumann U, Steinmetz I. Role of inducible nitric oxide synthase and NADPH oxidase in early control of *Burkholderia pseudomallei* infection in mice. *Infection and immunity*. 2006; 74:6300–6309. [PubMed: 17000727]

13. Koh GC, Maude RR, Schreiber MF, Limmathurotsakul D, Wiersinga WJ, Wuthiekanun V, Lee SJ, Mahavanakul W, Chaowagul W, Chierakul W, White NJ, van der Poll T, Day NP, Dougan G, Peacock SJ. Glyburide is anti-inflammatory and associated with reduced mortality in melioidosis. *Clinical infectious diseases : an official publication of the Infectious Diseases Society of America*. 2011; 52:717–725. [PubMed: 21293047]
14. Koh GC, Schreiber MF, Bautista R, Maude RR, Dunachie S, Limmathurotsakul D, Day NP, Dougan G, Peacock SJ. Host responses to melioidosis and tuberculosis are both dominated by interferon-mediated signaling. *PloS one*. 2013; 8:e54961. [PubMed: 23383015]
15. Pankla R, Buddhisa S, Berry M, Blankenship DM, Bancroft GJ, Banchereau J, Lertmemongkolchai G, Chaussabel D. Genomic transcriptional profiling identifies a candidate blood biomarker signature for the diagnosis of septicemic melioidosis. *Genome biology*. 2009; 10:R127. [PubMed: 19903332]
16. Chin CY, Monack DM, Nathan S. Genome wide transcriptome profiling of a murine acute melioidosis model reveals new insights into how *Burkholderia pseudomallei* overcomes host innate immunity. *BMC genomics*. 2010; 11:672. [PubMed: 21110886]
17. Chaussabel D, Quinn C, Shen J, Patel P, Glaser C, Baldwin N, Stichweh D, Blankenship D, Li L, Munagala I, Bennett L, Allantaz F, Mejias A, Ardura M, Kaizer E, Monnet L, Allman W, Randall H, Johnson D, Lanier A, Punaro M, Wittkowski KM, White P, Fay J, Klintmalm G, Ramilo O, Palucka AK, Banchereau J, Pascual V. A modular analysis framework for blood genomics studies: application to systemic lupus erythematosus. *Immunity*. 2008; 29:150–164. [PubMed: 18631455]
18. Kang MJ, Yoon CM, Nam M, Kim DH, Choi JM, Lee CG, Elias JA. Role of Chitinase 3-like-1 in IL-18-induced Pulmonary Type-1, -2 and -17 Inflammation, Alveolar Destruction and Airway Fibrosis in the Murine Lung. *Am J Respir Cell Mol Biol*. 2015
19. Duffield JS, Lupher M, Thannickal VJ, Wynn TA. Host responses in tissue repair and fibrosis. *Annu Rev Pathol*. 2013; 8:241–276. [PubMed: 23092186]
20. Santanirand P, Harley VS, Dance DA, Drasar BS, Bancroft GJ. Obligatory role of gamma interferon for host survival in a murine model of infection with *Burkholderia pseudomallei*. *Infection and immunity*. 1999; 67:3593–3600. [PubMed: 10377144]
21. Tippayawat P, Saenwongsa W, Mahawantung J, Suwannasaen D, Chetchotisakd P, Limmathurotsakul D, Peacock SJ, Felgner PL, Atkins HS, Titball RW, Bancroft GJ, Lertmemongkolchai G. Phenotypic and functional characterization of human memory T cell responses to *Burkholderia pseudomallei*. *PLoS neglected tropical diseases*. 2009; 3:e407. [PubMed: 19352426]
22. Berry MP, Graham CM, McNab FW, Xu Z, Bloch SA, Oni T, Wilkinson KA, Banchereau R, Skinner J, Wilkinson RJ, Quinn C, Blankenship D, Dhawan R, Cush JJ, Mejias A, Ramilo O, Kon OM, Pascual V, Banchereau J, Chaussabel D, O'Garra A. An interferon-inducible neutrophil-driven blood transcriptional signature in human tuberculosis. *Nature*. 2010; 466:973–977. [PubMed: 20725040]
23. Bloom CI, Graham CM, Berry MP, Rozakeas F, Redford PS, Wang Y, Xu Z, Wilkinson KA, Wilkinson RJ, Kendrick Y, Devouassoux G, Ferry T, Miyara M, Bouvry D, Valeyre D, Gorochov G, Blankenship D, Saadatian M, Vanhems P, Beynon H, Vancheeswaran R, Wickremasinghe M, Chaussabel D, Banchereau J, Pascual V, Ho LP, Lipman M, O'Garra A. Transcriptional blood signatures distinguish pulmonary tuberculosis, pulmonary sarcoidosis, pneumonias and lung cancers. *PloS one*. 2013; 8:e70630. [PubMed: 23940611]
24. Wiersinga WJ, Dessing MC, van der Poll T. Gene-expression profiles in murine melioidosis. *Microbes and infection / Institut Pasteur*. 2008; 10:868–877. [PubMed: 18653369]
25. Easton A, Haque A, Chu K, Lukaszewski R, Bancroft GJ. A critical role for neutrophils in resistance to experimental infection with *Burkholderia pseudomallei*. *The Journal of infectious diseases*. 2007; 195:99–107. [PubMed: 17152013]
26. Wiersinga WJ, Wieland CW, Dessing MC, Chantratita N, Cheng AC, Limmathurotsakul D, Chierakul W, Leendertse M, Florquin S, de Vos AF, White N, Dondorp AM, Day NP, Peacock SJ, van der Poll T. Toll-like receptor 2 impairs host defense in gram-negative sepsis caused by *Burkholderia pseudomallei* (Melioidosis). *PLoS medicine*. 2007; 4:e248. [PubMed: 17676990]
27. Ingersoll SA, Laval J, Forrest OA, Preininger M, Brown MR, Arafat D, Gibson G, Tangpricha V, Tirouvanziam R. Mature cystic fibrosis airway neutrophils suppress T cell function: evidence for a

- role of arginase 1 but not programmed death-ligand 1. *J Immunol.* 2015; 194:5520–5528. [PubMed: 25926674]
28. Munder M. Arginase: an emerging key player in the mammalian immune system. *Br J Pharmacol.* 2009; 158:638–651. [PubMed: 19764983]
29. Munder M, Choi BS, Rogers M, Kropf P. L-arginine deprivation impairs *Leishmania* major-specific T-cell responses. *European journal of immunology.* 2009; 39:2161–2172. [PubMed: 19637195]
30. Modolell M, Choi BS, Ryan RO, Hancock M, Titus RG, Abebe T, Hailu A, Muller I, Rogers ME, Bangham CR, Munder M, Kropf P. Local suppression of T cell responses by arginase-induced L-arginine depletion in nonhealing leishmaniasis. *PLoS neglected tropical diseases.* 2009; 3:e480. [PubMed: 19597544]
31. Seok J, Warren HS, Cuenca AG, Mindrinos MN, Baker HV, Xu W, Richards DR, McDonald-Smith GP, Gao H, Hennessy L, Finnerty CC, Lopez CM, Honari S, Moore EE, Minei JP, Cuschieri J, Bankey PE, Johnson JL, Sperry J, Nathens AB, Billiar TR, West MA, Jeschke MG, Klein MB, Gamelli RL, Gibran NS, Brownstein BH, Miller-Graziano C, Calvano SE, Mason PH, Cobb JP, Rahme LG, Lowry SF, Maier RV, Moldawer LL, Herndon DN, Davis RW, Xiao W, Tompkins RG. Genomic responses in mouse models poorly mimic human inflammatory diseases. *Proceedings of the National Academy of Sciences of the United States of America.* 2013; 110:3507–3512. [PubMed: 23401516]

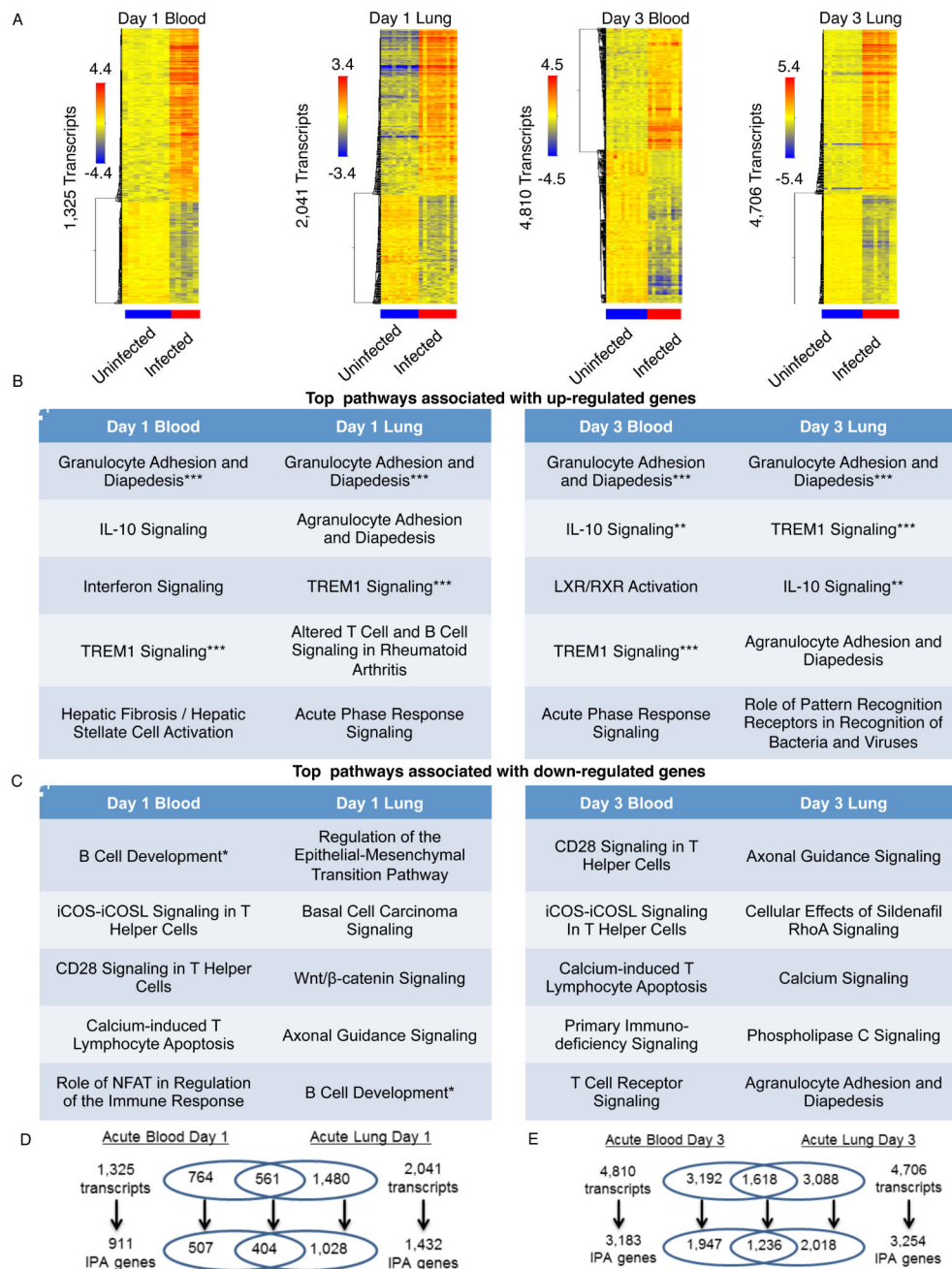


**Fig. 1. Mouse blood and lung transcriptional signatures are associated with similar and distinct canonical pathways after acute *B. pseudomallei* infection**

A. Heatmaps of normalized expression values of blood day 1 (infected n=5, uninfected n=8), lung day1 (infected/uninfected n=10), blood day 3 (infected n=9, uninfected n=11) and lung day 3 (infected n=9, uninfected n=10) differentially expressed transcripts. Scale bar represents log<sub>2</sub> fold change of up (red) or downregulated (blue) transcripts. See also Fig. S1. B, C. Top 5 significant Ingenuity Pathway Analysis (IPA) pathways ( $p < 0.01$  after Fisher's Exact Test) associated with up- or downregulated transcripts found within the 1325 blood day 1; 2041 lung day 1; 4810 blood day 3 and 4706 lung day 3 differentially expressed

transcripts are shown. Canonical pathways that are common to day 1 blood and lung, to day 3 blood and lung, and to the four datasets are denoted by one, two and three asterisks, respectively.

D, E. Venn diagram showing the number of overlapping transcripts between blood and lung transcriptional signatures.

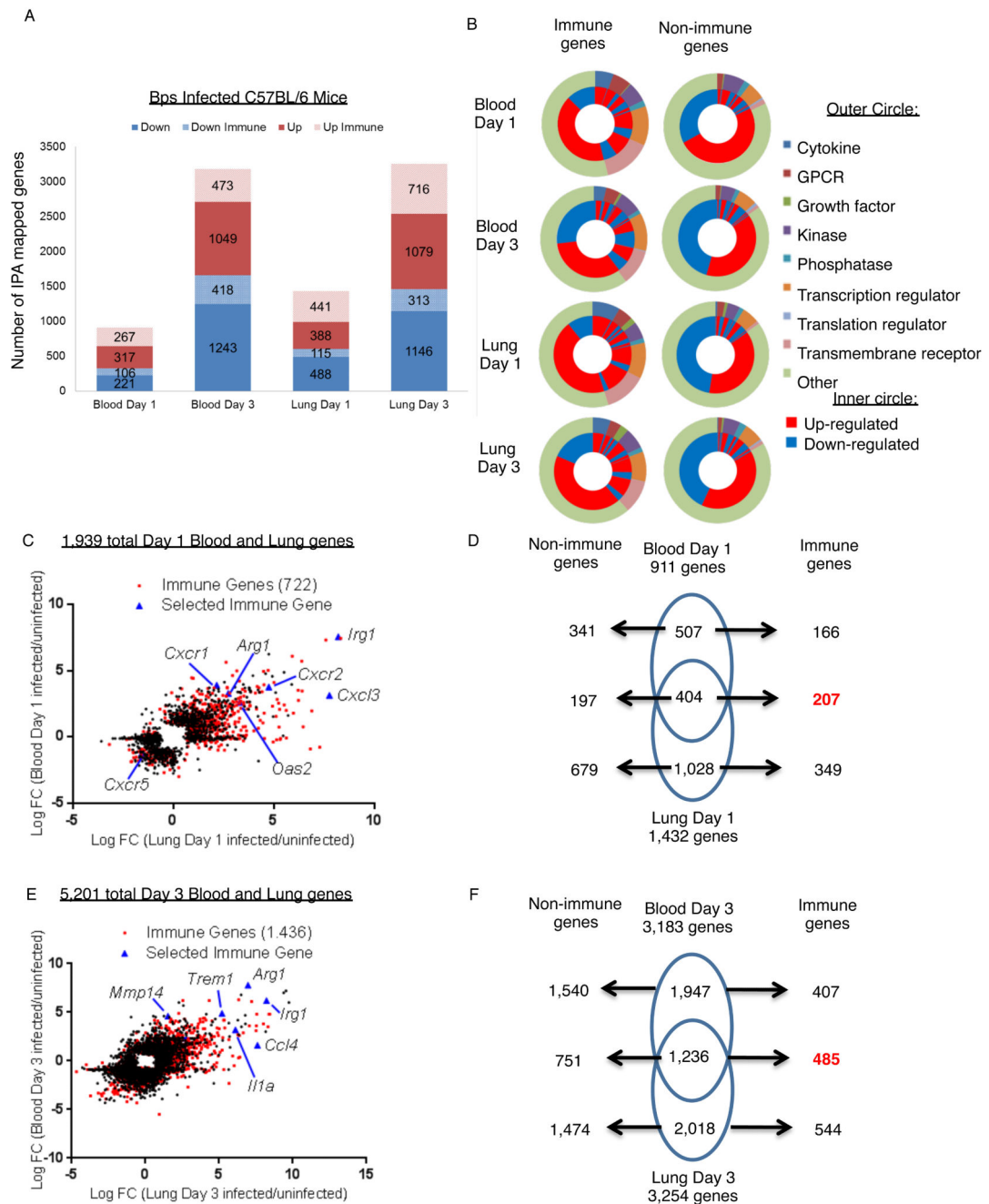


**Fig. 2. Immune genes are associated with blood and lung transcriptional signatures following acute *B. pseudomallei* infection**

A. Bar chart of the immune and nonimmune gene distribution within the 911 blood day 1 genes, 3183 blood day 3 genes, 1432 lung day 1 genes and 3254 lung day 3 genes.

B. Two layer donut chart showing the functional annotation of down, down immune, up and up immune genes found within blood day 1, blood day 3, lung day 1 and lung day 3 genes.

C. Scatter plot of total blood and lung genes at day 1 derived by combining 911 blood day 1 and 1432 lung day 1 differentially expressed genes. 722 Immune genes are marked in red.

- D. Venn diagram showing the common and dataset-specific genes for blood and lung at day 1 post infection. The number of immune and nonimmune genes is indicated.
- E. Scatter plot of total blood and lungs genes at day 3 derived by combining 3183 blood day 3 and 3254 lung day 3 differentially expressed genes. 1436 Immune genes are marked in red.
- F. Venn diagram showing the common and dataset-specific immune versus nonimmune genes for blood and lung at day 3 post infection.

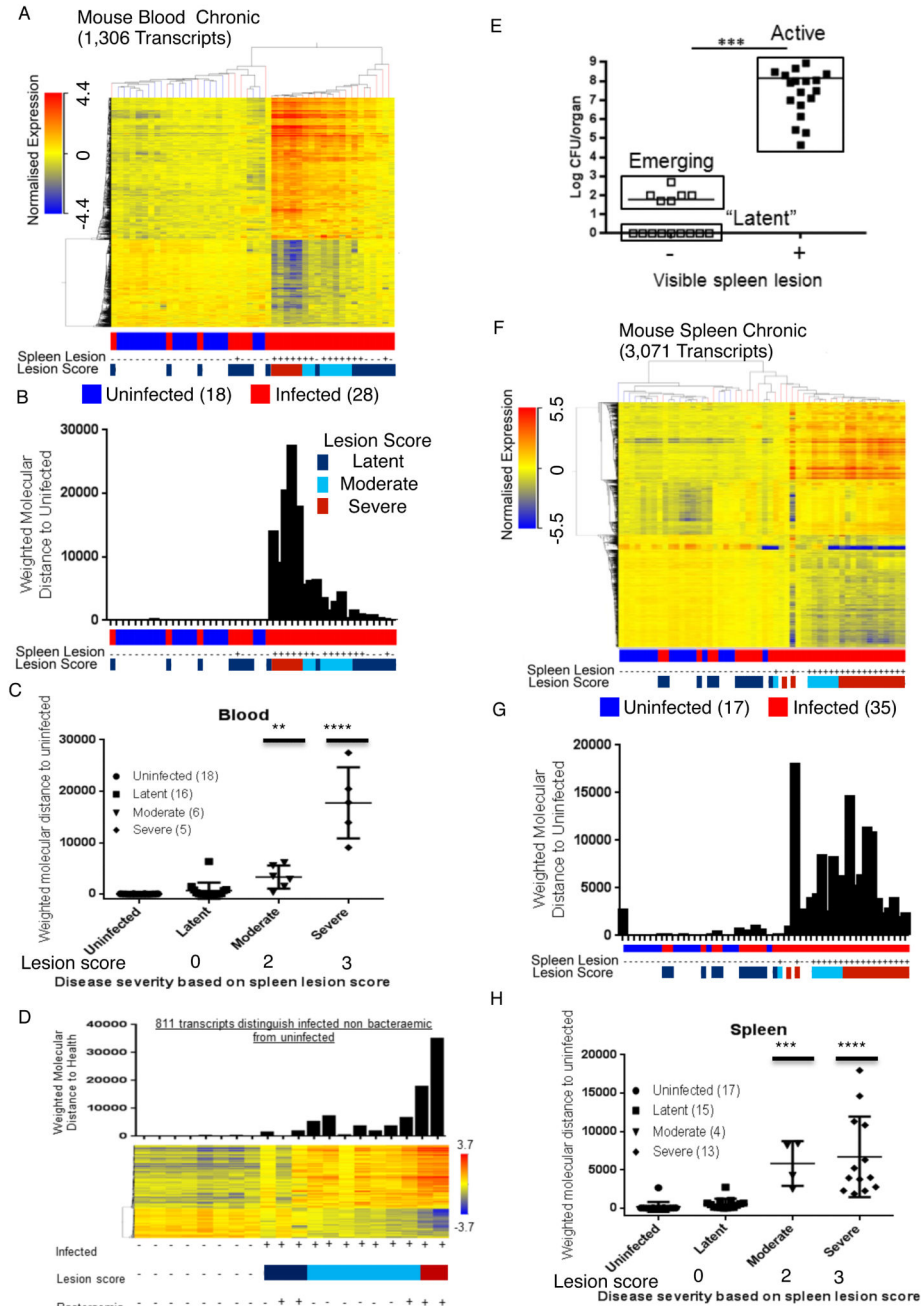


**Fig. 3. Mouse blood and spleen transcriptional signatures following chronic *B. pseudomallei* infection reveal differences in latent versus active disease state**

(A, F) Unsupervised clustering based heatmaps of normalized expression values of blood chronic (infected n=28, uninfected n=18) and spleen chronic (infected n=35, uninfected n=17) differentially expressed transcripts. Scale bar represents log<sub>2</sub> fold change of up (red) or downregulated (blue) transcripts. See also Fig. S1.

(B, G) Molecular distance to health/uninfected (MDTH) is aligned against the hierarchical condition tree generated through unsupervised clustering (top).

(C, H) Correlation of individual MDTH to lesion severity score. Horizontal bars represent the median value for each group.

(D) Heatmap of 811 significant transcripts that were identified by comparing *B. pseudomallei* infected mice without bacteraemia (n=7) to uninfected (n=8). Lesion scores were applied to generate a supervised heatmap of the identified transcripts.

(E) Bacterial counts from spleens were allocated in two groups according to the presence or absence of visible lesions. Each symbol represents an individual organ. The horizontal line represents the mean  $p < 0.001$  (\*\*\*) between mice with or without visible lesions. Scale bar represents log<sub>2</sub> fold change of up (red) or downregulated (blue) transcripts (A, D, F).

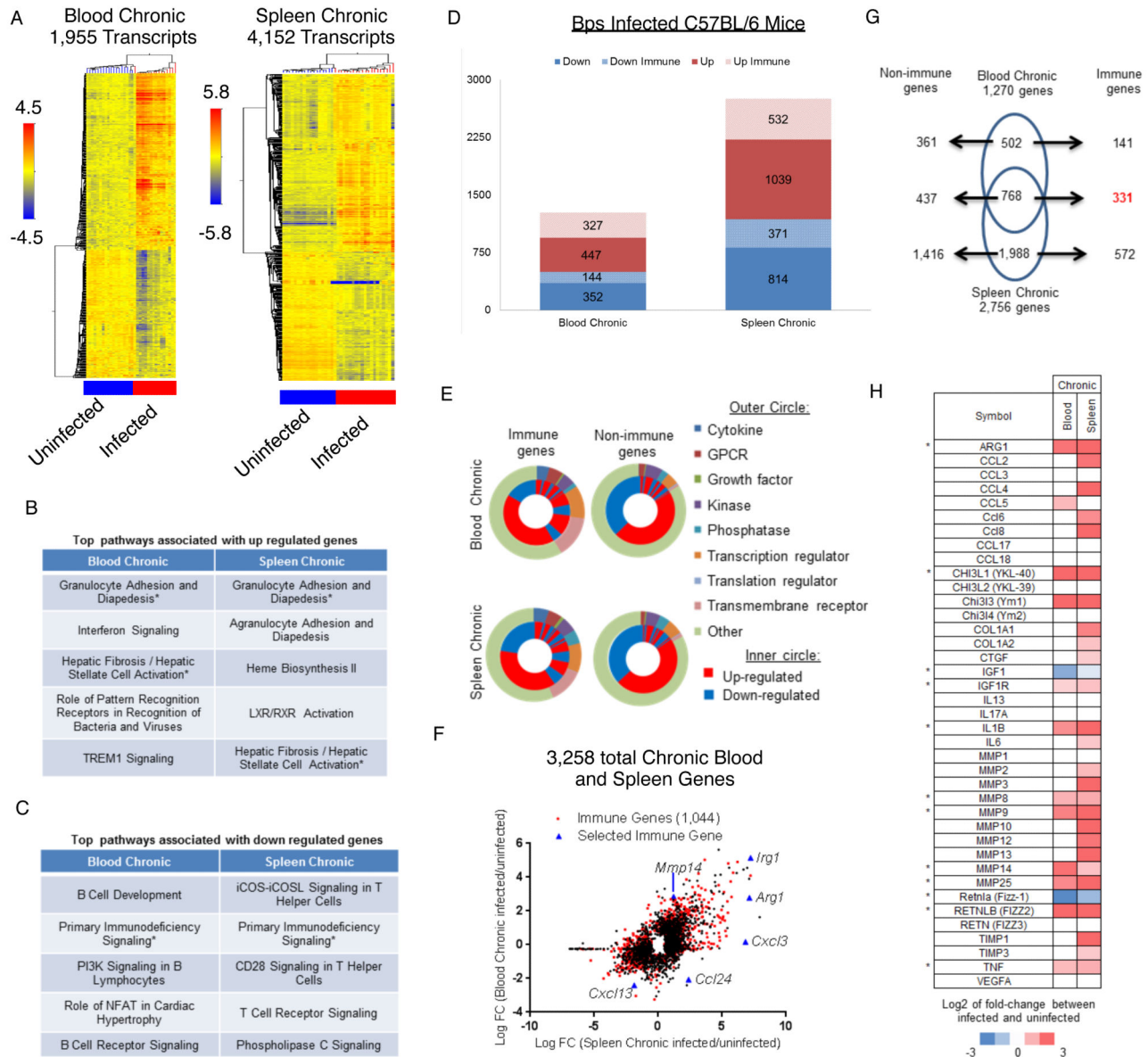


**Fig. 4. Similar and distinct canonical pathways and immune genes are associated with blood and spleen transcriptional signatures in active chronic *B. pseudomallei* disease**

A. Heatmaps of uninfected versus active chronic infected mice showing unsupervised clustering of 1955 blood chronic (infected n=16, uninfected n=18) and 4152 spleen chronic (infected n=20, uninfected n=17) differentially expressed transcripts. Scale bar represents log<sub>2</sub> fold change of up (red) or down (blue) regulated transcripts.

B, C. Ingenuity Pathway Analysis (IPA) of the up- or down-regulated transcripts found within the 1955 blood chronic and 4152 spleen chronic differentially expressed transcripts shows the top 5 significant canonical pathways ( $p < 0.01$  after Fisher's Exact Test). Pathways that are common to both datasets are marked with a single asterisk.

D. Bar chart summarizing the immune and nonimmune gene distribution within the 1955 blood and 4152 spleen transcripts that map to 1270 and 2756 active chronic blood and chronic spleen genes.

E. Two layer donut chart showing the functional annotation of down, down immune, up and up immune genes found within 1270 blood and 2756 spleen genes in active chronic infection.

F. Scatter plot of total blood and spleen genes in active chronic infection derived by combining the 1270 blood and 2756 spleen genes. A list of 1044 Immune genes identified within the 3258 total blood-spleen genes by searching the IPA Knowledge Base and Gene Ontology resources available through MGD are marked in red.

G. Venn diagram showing the common and dataset-specific immune versus nonimmune genes for blood and spleen in active chronic infection. See also Fig. S2 for gene lists.

H. Intensity plot of 39 fibrosis genes across *B. pseudomallei* infected mouse chronic blood and spleen datasets listed above. Scale bar represents log<sub>2</sub> fold change of up- (red) or downregulated (blue) genes. Asterisks highlight immune genes that are common to chronic blood and spleen.

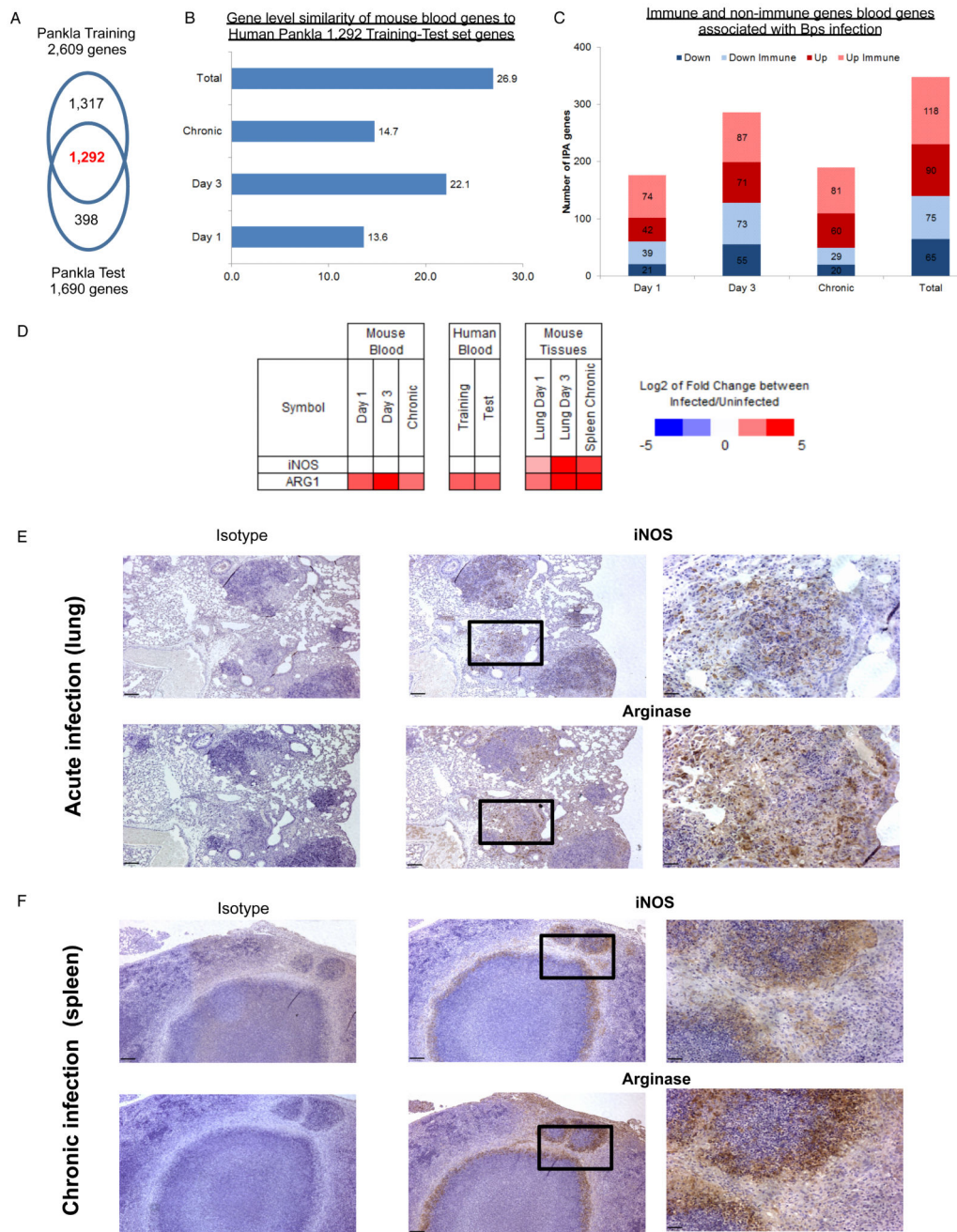


**Fig. 5. Gene level and histology analysis of transcriptional signatures common to mouse-human following *B. pseudomallei* infection**

A. Venn diagram shows 1292 overlapping genes between the Pankla Training and the Pankla Test set differentially expressed genes. The significant gene lists were identified by stringent statistical filtering comparing blood from diseased individuals to those from healthy controls (Mann-Whitney test plus Benjamini-Hochberg correction  $p < 0.01$ ) on data normalized to the median of all transcripts across all samples and passing a detection value ( $p < 0.01$ ) and 2-fold expression value across at least 10% of samples within GeneSpring GX12.1 statistical software.

B. Percentage similarity of mouse blood *B. pseudomallei* infection-associated datasets to human blood 1292 Pankla gene list. The percentages range from 13.6 to 26.9% with day 1 (13.6%), day 3 (22.1%), Chronic (14.7%) and Total (26.9%) mouse similarity to human Pankla 1292 gene list.

C. Bar chart summarizing the immune and nonimmune gene distribution within 176 day 1, 286 day 3, 190 Chronic and 348 Total mouse-human blood genes associated with *B. pseudomallei* infection.

D. Intensity plot shows the expression of *iNos* and *Arg1* genes across mouse and human datasets.

E,F. Immunohistochemical staining for iNOS and Arginase-1 (centre and right columns) of lung (E) and spleen (F) sections from mice, following an acute (day 3) or chronic infection (day 21), respectively. Left columns show isotype controls. Magnified microphotographs on the right show iNOS and Arginase-1 staining from insets in the central columns. Scale bar: 140 um (left and central columns) and 36 um right column.

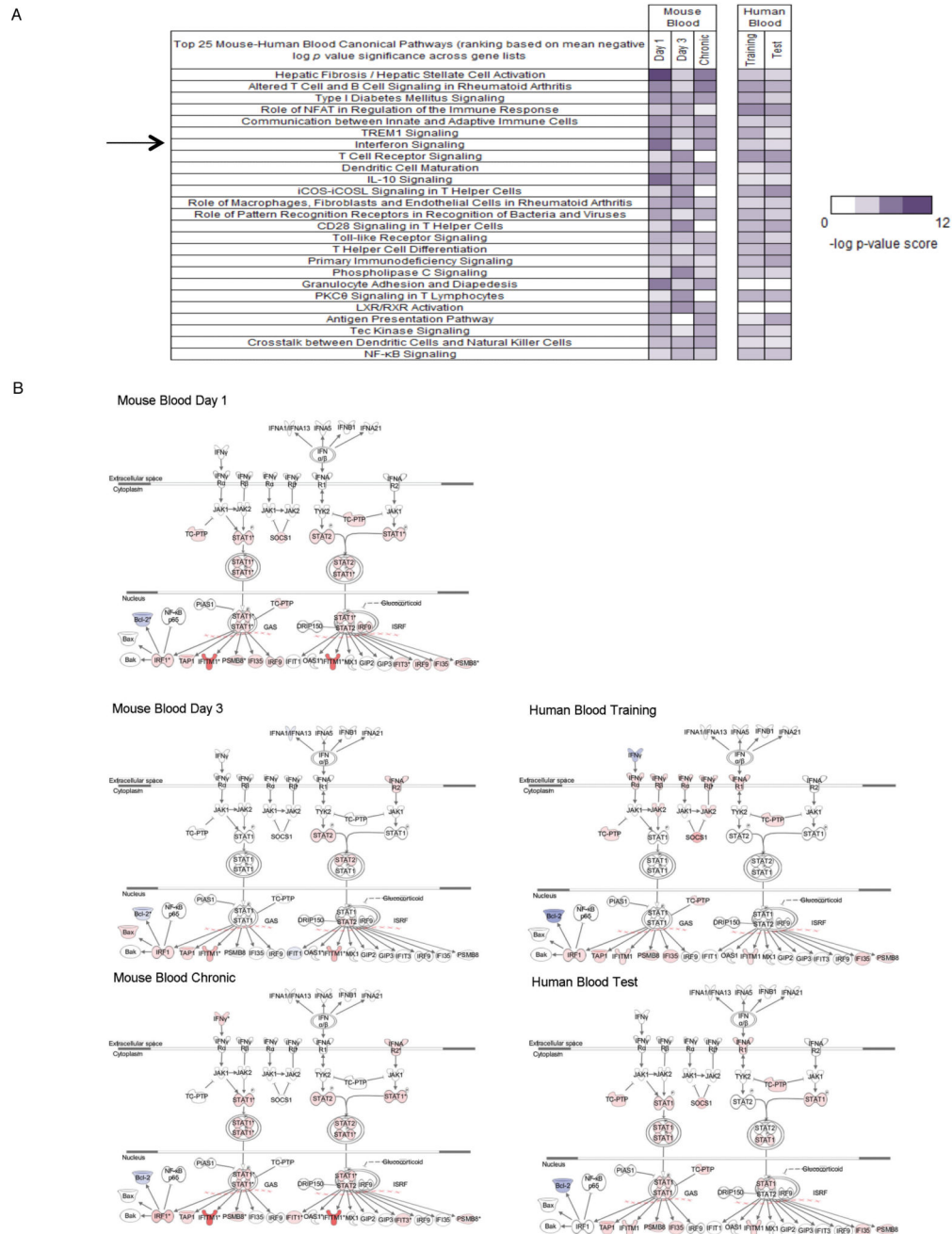


**Fig. 6. Immune pathways including IFN-signaling are significantly associated with mouse and human blood transcriptional signatures after *B. pseudomallei* infection**

A. Top 25 ranked pathways across human and mouse blood datasets after *B. pseudomallei* infection based on their average *p*-value. Arrow indicated the IFN canonical signaling pathway shown in B. See also Fig. S3 for IPA top10 pathways associated with each dataset.

B. Graphical representation for mouse and human blood canonical IFN-signaling pathway found within IPA. Fold-change of up- and down-regulated genes are indicated with red and blue shading.

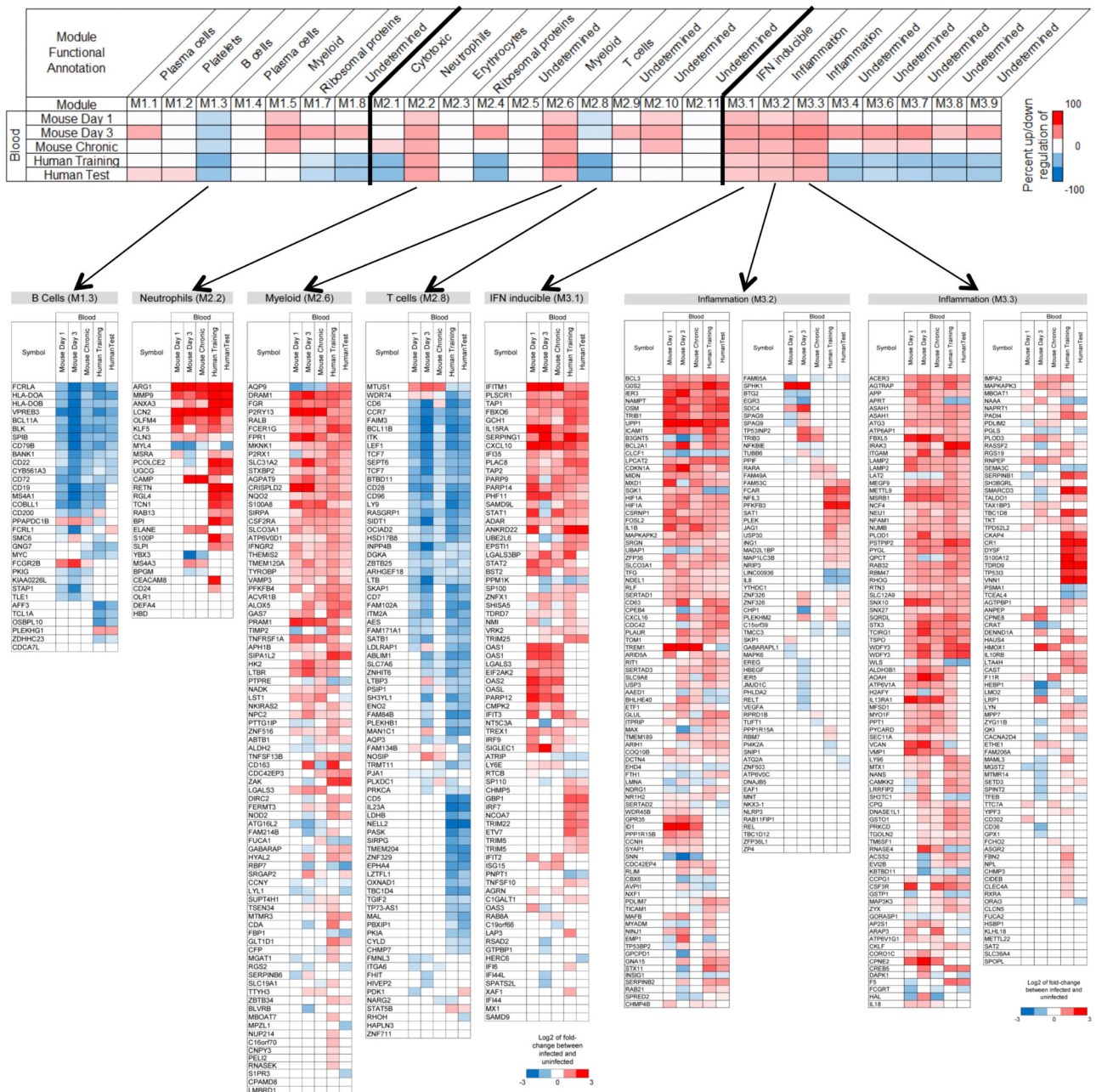


**Fig. 7. Modular analysis of blood transcriptional profiles reveals a degree of similarity between mouse and human datasets**

Heatmap summary of significant up- or downregulation in modules associated with *B. pseudomallei* mouse and human datasets and passing a  $p$ -value  $<0.05$  after  $t$ -test comparing infected to uninfected groups (top). Gene-level analysis of modules that are common across the five datasets are detailed from left to right B cell (M1.3), Neutrophils (M2.2), Myeloid (M2.6), T-cell (M2.8), and IFN Inducible (M3.1); Inflammation (M3.2) and Inflammation (M3.3). Scale bar represents log<sub>2</sub> fold change of up (red) or down (blue) regulated genes.

179 directly interacting from the 348 Total Mouse-Human Genes

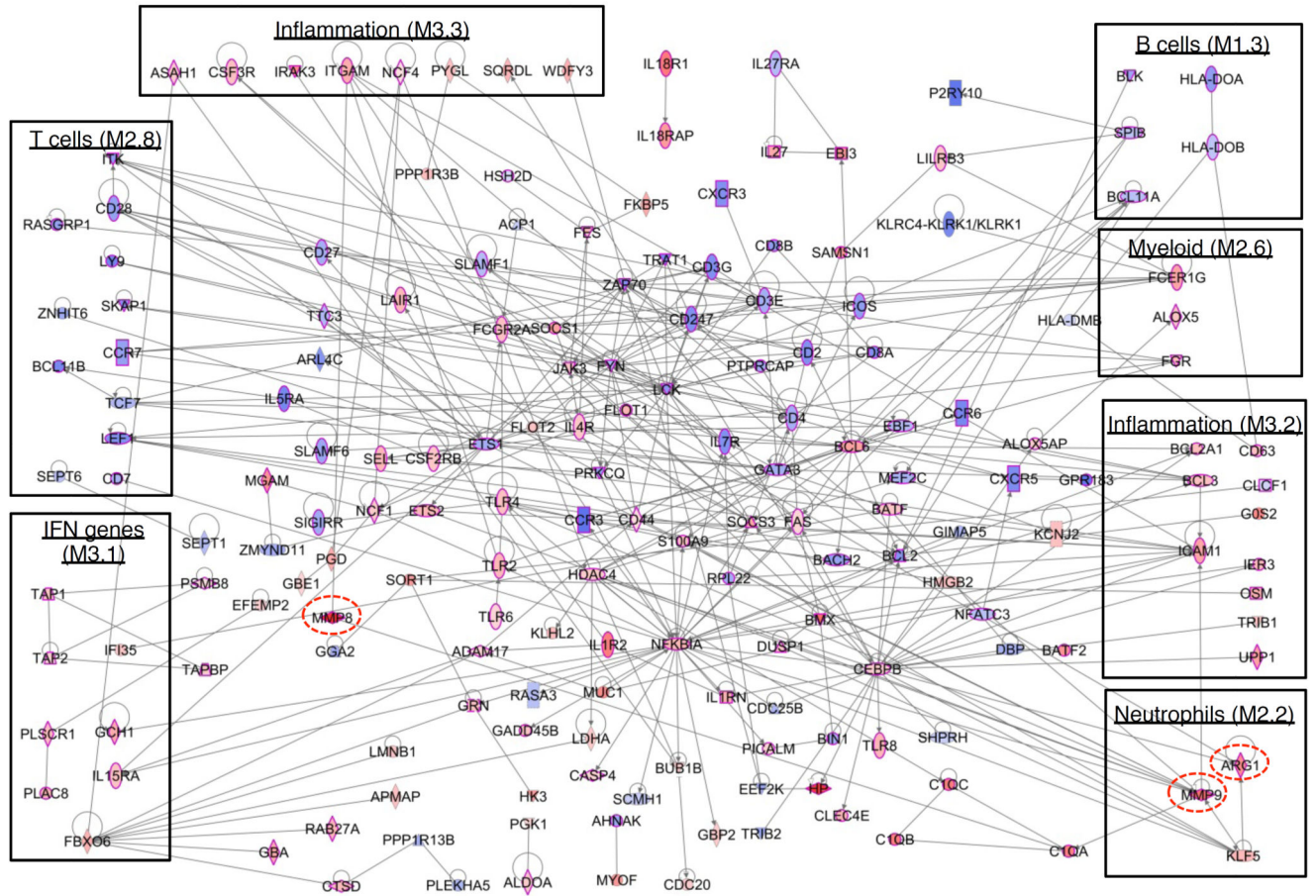


**Fig. 8. Network level analysis of common mouse-human *B. pseudomallei* associated transcriptional signatures**

IPA network between 179 of the 348 Total mouse-human blood genes. Genes found within modules detailed in Fig. 7 are boxed, while 130 genes associated with an immune function are bordered in red. Fold change for up- and down-regulated genes is indicated with red and blue shading, respectively. Dotted circles highlight immune fibrosis genes also seen in Figs. 4H and S2.